Materials Chemistry and Physics 136 (2012) 439–447

Contents lists available at SciVerse ScienceDirect

Materials Chemistry and Physics

journal homepage: www.elsevier.com/locate/matchemphys

Preparation, characterization, photocatalytic activity and conductivity of $BiLnZr_2O_7$ (Ln = La, Sm, Eu and Gd)

B. Vijaya Kumar [a,d], Radha Velchuri [a], G. Prasad [b], C. Bansal [c], M. Vithal [a,*]

[a] Department of Chemistry, Osmania University, Hyderabad 500 007, India
[b] Department of Physics, Osmania University, Hyderabad 500 007, India
[c] School of Physics, University of Hyderabad, Hyderabad 500 134, India
[d] Department of Chemistry, National Institute of Technology, Warangal 506 004, India

HIGHLIGHTS

- $BiLnZr_2O_7$ (Ln = La, Sm, Eu, Gd) were prepared by sol–gel method.
- $BiLnZr_2O_7$ (Ln = Sm, Eu) are unstable above 700 °C.
- These pyrochlores show good photoactivity in the presence of H_2O_2.

ARTICLE INFO

Article history:
Received 19 January 2012
Received in revised form
1 July 2012
Accepted 5 July 2012

Keywords:
A. Oxides
B. Sol–gel growth
C. TGA
D. Electrical conductivity

ABSTRACT

Bismuth containing pyrochlore type oxides ($BiLnZr_2O_7$; Ln = La, Sm, Eu and Gd) were prepared by sol–gel method. The obtained compositions were characterized by powder X-ray diffraction (PXRD), Thermal analysis (DTA–TG), Raman spectroscopy, Energy dispersive spectroscopy (EDS) and UV–Vis diffuse reflectance spectroscopy (DRS). Both $BiSmZr_2O_7$ and $BiEuZr_2O_7$ are unstable above 700 °C unlike $BiLaZr_2O_7$ and $BiGdZr_2O_7$. All the samples show good photocatalytic activity under visible light irradiation in presence of H_2O_2. The DC conductivity of all these materials was carried out in the temperature range 130–700 °C and a detailed explanation for the observed changes is given.

© 2012 Elsevier B.V. All rights reserved.

1. Introduction

Pyrochlore type oxides of general formula $A_2B_2O_7$ or more appropriately $A_2B_2O_6O'$ to indicate the interpenetrating network of tetrahedral A_2O' with corner sharing B_2O_6 octahedra, have been extensively studied [1]. These oxides crystallize in cubic lattice with $Fd\bar{3}m$ space group. Eight coordinate A site can be occupied by trivalent lanthanides, divalent alkaline earth or monovalent alkali ions. Site B can be filled by six coordinate tetravalent (Ti^{4+}, Zr^{4+}, Hf^{4+}or Sn^{4+}) or pentavalent (Nb^{5+}, Ta^{5+}) ions for charge neutrality. The A and B cations occupy 16d and 16c sites respectively with $\bar{3}m$ symmetry. The oxygen ions occupy 48f (x, 1/8, 1/8) with $2mm$ symmetry while O′ occupies 8b site having $\bar{4}3m$ symmetry. Site 8a is systematically vacant. The ordered pyrochlore structure is a super structure of defect fluorite ($Fm\bar{3}m$ space group) with twice the lattice constant [1]. It is observed that ideal defect fluorite structure is seldom obtained due to the presence of anion vacancies and short range ordering of A and B cations. The 48f position of oxygen is displaced and its magnitude is given by positional parameter, *x*, which is found to be in the range 0.3125–0.375 for the pyrochlore structure. Pyrochlore oxides containing polarizable "A" cations have been the subject of considerable interest. These insulating electro ceramic oxides are considered as materials for capacitor and high frequency filter applications due to their high dielectric constants, low dielectric loss and tunable temperature coefficients [2]. These oxides possessing A cations with lone pair of electrons such as Bi^{3+} or Sn^{2+} exhibit disorder in the A_2O' network which is due to static displacements at this site [3]. The space to accommodate the active lone pair of electrons of A cation ($\bar{3}m$ symmetry) in the puckered hexagonal ring of oxygen atoms is limited. The mixing of Bi 6s-M d orbitals reduces the lone pair character of Bi^{3+} leading to stable pyrochlore phases, $Bi_2M_2O_7$ (M = Rh, Ru, Ir) [4,5]. Pyrochlore materials containing bismuth have

* Corresponding author. Tel.: +91 40 276823237; fax: +91 40 27090020.
E-mail addresses: mugavithal@gmail.com, muga_vithal@osmania.ac.in (M. Vithal).

0254-0584/$ – see front matter © 2012 Elsevier B.V. All rights reserved.
http://dx.doi.org/10.1016/j.matchemphys.2012.07.005

potential applications for low-fire high frequency devices due to their low sintering temperatures (<950 °C), high quality factor (φ = (dielectric loss^{-1})) and controllable temperature coefficient of capacitance (TCC) [6,7]. Further, Bi^{3+} containing $A_2B_2O_7$ oxides have been used to improve the electrical characteristics of $Bi_4Ti_3O_{12}$ [8] and PZT [9] ferroelectric thin films and are potential gate materials for advanced metal oxide semiconductor (MOS) transistors [10]. The studies pertaining to photocatalytic activity of ternary $A_2B_2O_7$ type oxides with pyrochlore structure have been reported [11,12]. The ternary semiconducting oxides and/or nitrides based on d^0 and/or d^{10} configuration have been developed [13–18] as photocatalysts. However the photocatalytic studies related to quaternary oxides having pyrochlore structure with $4f^0$ and/or $3d^{10}$ configurations are scarce. To our knowledge, the systematic studies on $BiLnZr_2O_7$ (Ln = La, Sm, Eu and Gd) type materials are not reported. In the present investigation we report the preparation, characterization, photocatalytic activity and conductivity studies of $BiLaZr_2O_7$, $BiSmZr_2O_7$, $BiEuZr_2O_7$ and $BiGdZr_2O_7$.

2. Experimental

The rare earth oxides, Ln_2O_3 (Ln = La, Sm, Eu and Gd) (99%) (Indian Rare-Earth Limited Corporation (India)), bismuth nitrate (99.8%, SD Fine), zirconyl nitrate (Wilson Laboratories, Bombay) and ammonia solution (25%, AR grade, SD Fine) were used directly without further purification. Stoichiometric amount of Ln_2O_3 was dissolved in excess concentrated nitric acid to form rare earth nitrate ($Ln(NO_3)_3$). Excess nitric acid was removed by slow heating. About 25 ml of de-ionized water was added. Calculated amount of zirconyl nitrate and bismuth nitrate were dissolved in hot de-ionized water separately. $Ln(NO_3)_3$ solution was mixed with the bismuth nitrate aqueous solution with constant stirring. To this resultant solution zirconyl nitrate solution was added. Then chelating agent, citric acid, was added. The molar ratio of citric acid to metal ion was 2:1. The pH of the resultant metal citrate solution was adjusted to 6–7 by adding dilute ammonia solution drop wise. The solution was then slowly evaporated on a water bath till a viscous liquid was obtained. At this stage the gelating reagent, ethylene glycol, was added to the solution. The molar ratio of chelating and gelating reagents was 1.0:1.2. This mixture was heated on a hot plate/stirrer at 100 °C for 2–3 h with constant stirring. The temperature was increased to 160–180 °C at the onset of solidification. The ensuing porous solid mass was ground in an agate mortar using spectral grade acetone. The resultant yellow colored solid (named as "precursor") was heated in a muffle furnace at various temperatures (500–975 °C) for 5 h each. The compositions $BiLaZr_2O_7$, $BiSmZr_2O_7$, $BiEuZr_2O_7$ and $BiGdZr_2O_7$ are abbreviated as BLZ, BSZ, BEZ and BGZ respectively. The abbreviation followed by a three digit number refers to the temperature at which the material is obtained. For instance, BLZ 600 stands for the material obtained when the precursor of $BiLaZr_2O_7$ is heated at 600 °C for 5 h.

The phase characterization was carried out using an Shimadzu XRD 7000 powder diffractometer (Cu-Kα of wavelength 1.5406 Å) at room temperature. The scan speed is 2° min^{-1} in the 2θ range of 10–80°. Thermogravimetric analysis (TGA) and differential thermal analysis (DTA) were performed using Shimadzu differential thermal analyzer (DTG-60H) with a heating rate of 15 °C min^{-1}. Raman spectra were recorded using a 632.81 nm line from a He–Ne laser and the scattered light was analyzed using HORIBA JOBIN YVON HR800. The laser was focused to a spot of ~3 μm and a 10× lens was used for the collection of back scattered Raman signal. The diffuse reflectance spectra (DRS) were measured in the range 200–800 nm by Perkin Elmer Lambda 750 UV–Vis spectrophotometer using reflectance standard, $BaSO_4$. The photocatalytic activity of all the compounds was evaluated against the degradation of methyl orange (MO) dye in an aqueous solution under visible light irradiation. A 150 W tungsten lamp is used. The suspension was prepared by adding 50 mg of BLZ and 1 ml of 3% H_2O_2 in 50 ml of MO solution (10 mg L^{-1}). It was taken into a specially designed long neck (25 cm) 100 ml round bottom flask and stirred in the dark for 30 min to ensure an adsorption/desorption equilibrium prior to irradiation. At regular time intervals, 5 ml suspension was taken and filtered using 0.2 μm bore filters to remove suspended particulates. The absorbance of the filtrate was measured using UVIKON 923 UV–Vis spectrophotometer 465 nm, the λ_{max} of MO. The DC conductivity of all samples was measured in the temperature range 130–700 °C using a two probe method on the sintered pellets coated with silver paint on both sides. For this, a conventional sample holder and Kiethely electrometer 610 °C were used.

3. Results and discussion

3.1. Powder X-ray diffraction

The precursor of BLZ, BSZ, BEZ and BGZ were calcined at 500, 600, 700, 800 and 975 °C separately for 5 h each. The powder patterns of all the above compounds calcined at 500, 600, and 700 °C were characterized by broad background with the appearance of peaks in the 2θ range of 28–30°, 33–35°, 46–50° and 55–64°. The presence of broad base line in the powder patterns indicates the amorphous nature of the samples along with some crystalline phase. The room temperature powder patterns of BLZ calcined at 600, 700, 800 and 975 °C are shown in Fig. 1. The intensity of diffraction peaks of samples calcined at 500 °C was very low and hence not shown. The powder patterns of BLZ calcined at 800 and 975 °C are similar to that of $La_2Zr_2O_7$ [JCPDF: 73-0444] except the impurity peak corresponding to ZrO_2 (shown by * in Fig. 1) in the former which disappeared in the later. It is well known that $A_2B_2O_7$ type oxides crystallize in "ordered pyrochlore" (cubic, space group $Fd\bar{3}m$) or "defect fluorite" lattice (cubic, space group $Fm3m$) depending upon the relative ratio of A and B cations and/or

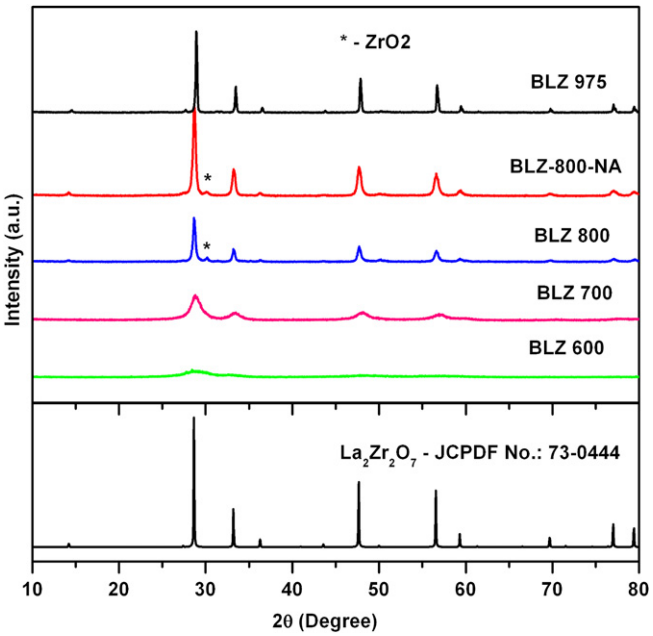

Fig. 1. Powder XRD patterns of BLZ calcined at different temperatures.

experimental conditions [19]. The observation of weak super lattice peaks at $2\theta \approx 14$–15, 27–28, 36 and 50° corresponding to (111), (311), (331) and (531) planes respectively in the powder patterns indicates the crystallization of $A_2B_2O_7$ in "ordered pyrochlore" lattice. These super lattice peaks are absent in these oxides with "defect fluorite" lattice. However, in some $A_2B_2O_7$ oxides with ordered pyrochlore lattice, the intensity of super lattice peaks is found to be too low to be observed by laboratory X-ray diffractometer. Thus the observation of super lattice peaks confirms the crystallization of oxides in the "ordered pyrochlore" lattice but its absence need not necessarily confirm the defect fluorite lattice. In the case of BLZ all the super lattice peaks were observed (Fig. 1). Therefore, it can be concluded that BLZ is crystallized in "ordered pyrochlore" lattice. This was further confirmed from its Raman spectrum given in the next section.

The powder patterns of BSZ and BEZ calcined at 600, 675 (24 h) 700, 800 and 975 °C are shown in Figs. 2 and 3 respectively. Fig. 4 shows powder patterns of BGZ calcined at 700 and 800 °C. Since all the bismuth compounds in the present investigation are derived from $Ln_2Zr_2O_7$ (Ln = Sm, Eu and Gd), a comparison of powder patterns with respective parent compounds is essential. $Sm_2Zr_2O_7$ is known to crystallize in ordered pyrochlore (JCPDF: 24-1012, $Sm_2Zr_2O_7$ (OP)) and defect fluorite (JCPDF: 78-1291, $Sm_2Zr_2O_7$ (DF)) lattices. Similarly, $Eu_2Zr_2O_7$ exists in ordered pyrochlore (JCPDF: 24-0418, $Eu_2Zr_2O_7$ (OP)) and defect fluorite (JCPDF: 78-1292, $Eu_2Zr_2O_7$ (DF)) lattices. $Gd_2Zr_2O_7$ is also known to crystallize in ordered pyrochlore (OP) and defect fluorite (JCPDF: 80-0471, $Gd_2Zr_2O_7$ (DF)) lattices depending on heat treatments [19]. The powder patterns of BSZ and BEZ (prepared at 600 and 700 °C) are similar to each other. It is difficult to judge the type of lattice adopted by BSZ and BEZ, prepared at these temperatures, from their powder patterns due to negligible intensity of super lattice peaks. But the Raman spectra of BSZ and BEZ (prepared at 700 °C), discussed in the next section, suggest that both BSZ and BEZ crystallize in the pyrochlore lattice. The powder XRDs of BGZ (calcined at 700 & 800 °C) are also similar to that of BSZ and BEZ patterns with negligible intensity for super lattice peaks. The Raman spectra of BGZ samples, however, indicate its crystallization in "defect fluorite" lattice.

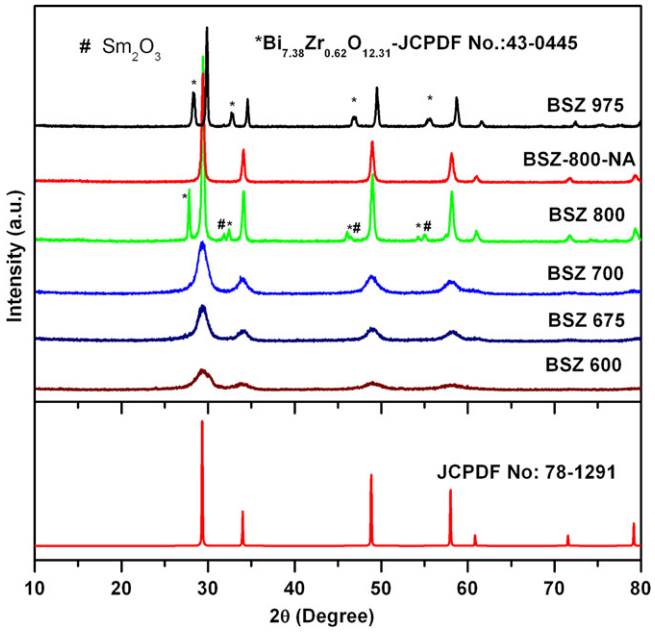

Fig. 2. Powder XRD patterns of BSZ calcined at different temperatures.

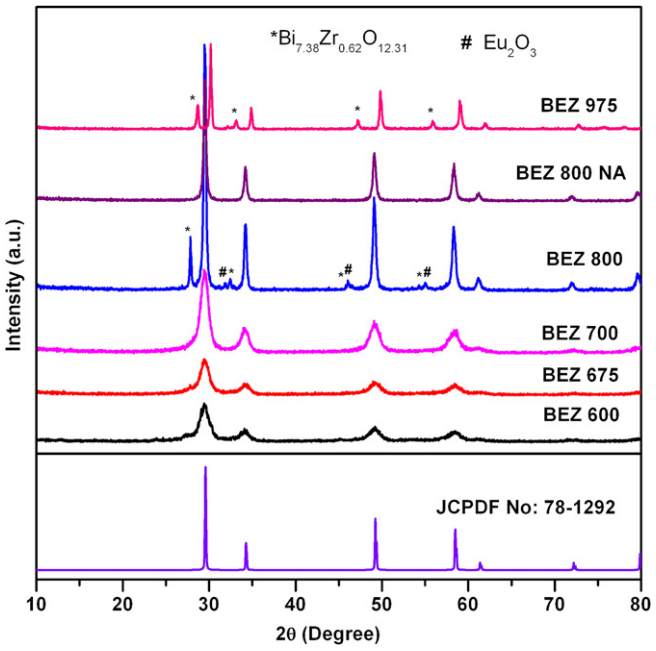

Fig. 3. Powder XRD patterns of BEZ calcined at different temperatures.

The powder patterns of BSZ and BEZ samples prepared at or above 800 °C were found to be quite different from those prepared at lower temperatures. These powder patterns were characterized by d-lines belonging to $Bi_{7.38}Zr_{0.62}O_{12.31}$ (JCPDF: 43-0445), $Ln_{0.2}Zr_{0.8}O_{1.9}$ [Ln = Sm and Eu ($Sm_{0.2}Zr_{0.8}O_{1.9}$; JCPDF: 78-1302 and

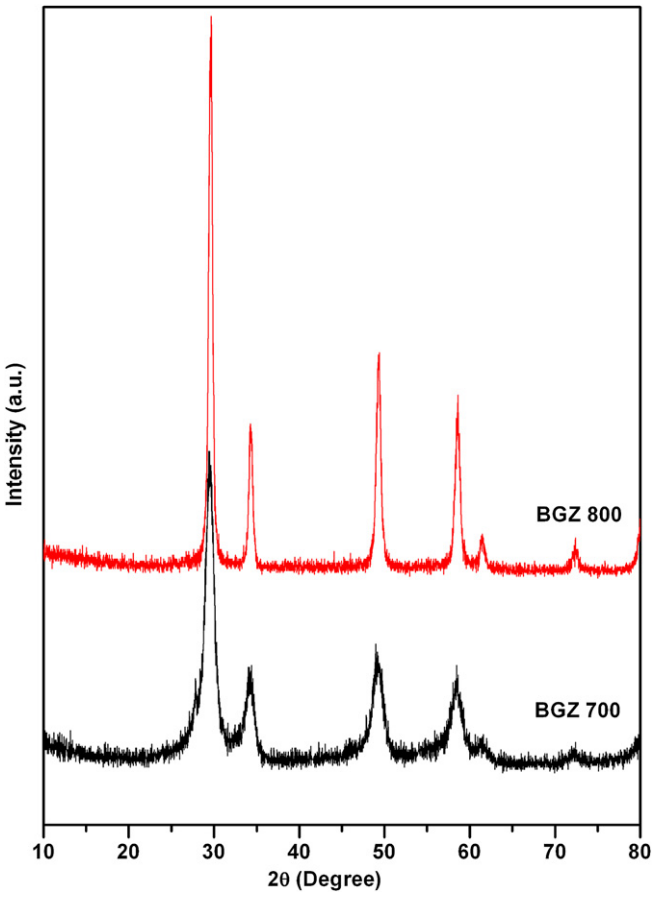

Fig. 4. Powder XRD patterns of BGZ calcined at different temperatures.

Table 1
The crystallite size (nm) of BLZ, BSZ, BEZ and BGZ at different temperatures.

Compound	Temperature (°C)	Crystallite size (nm)
BLZ	700	6.00
	800	22.00
BSZ	700	6.17
	800	27.00
BEZ	700	7.53
	800	24.2
BGZ	800	21.3

$Eu_{0.2}Zr_{0.8}O_{1.9}$; JCPDF: 78-1303)] and Ln_2O_3 (Ln = Sm and Eu (Sm_2O_3; JCPDF: 86-2479) and (Eu_2O_3; JCPDF: 86-2476)) phases. We believe that $BiLnZr_2O_7$ is decomposed to $Bi_{7.38}Zr_{0.62}O_{12.31}$, $Ln_{0.2}Zr_{0.8}O_{1.9}$ and Ln_2O_3 (Ln = Sm and Eu). The sintering temperature for both BSZ and BEZ was increased to 975 °C to know further decomposition of $Bi_{7.38}Zr_{0.62}O_{12.31}$ and $Ln_{0.2}Zr_{0.8}O_{1.9}$ phases. The powder patterns of these samples (sintered at 975 °C for 5 h) are similar to those observed for samples heated at 800 °C. Thus it can be concluded that both BSZ and BEZ decompose at 800 °C to $Bi_{7.38}Zr_{0.62}O_{12.31}$, $Ln_{0.2}Zr_{0.8}O_{1.9}$ and Ln_2O_3. Both $Bi_{7.38}Zr_{0.62}O_{12.31}$ and $Ln_{0.2}Zr_{0.8}O_{1.9}$ are stable up to 975 °C. Similar results were observed in the case of $Bi_2Ti_2O_7$ [20]. Since the products obtained at or above 800 °C were mixtures containing $Bi_{7.38}Zr_{0.62}O_{12.31}$, $Ln_{0.2}Zr_{0.8}O_{1.9}$ and Ln_2O_3, they were washed with concentrated HNO_3. The undissolved solid (indicated as BLnZ-800-NA (Ln = Sm, Eu)) gave d-lines belonging to $Ln_{0.2}Zr_{0.8}O_{1.9}$ phase (fluorite lattice) only. The filtrate was tested positive for Bi^{3+} [21]. Thus the possible reaction is

$$7.38BiLnZr_2O_7(Ln = Sm\ and\ Eu) \xrightarrow{800^{\circ}C} Bi_{7.38}Zr_{0.62}O_{12.31} + 17.675Ln_{0.2}Zr_{0.8}O_{1.9} + 1.9225Ln_2O_3 \xrightarrow{Conc.HNO_3} Ln_{0.2}Zr_{0.8}O_{1.9} + filtrate$$

All the observed diffraction peaks for BSZ, BEZ and BGZ calcined up to 700 °C are broad indicating the nano nature of the material. The crystallite sizes were calculated from the line width of intense line using Scherer's formula [22] and are given in Table 1.

3.2. Thermal analysis (DTA–TG)

Differential thermal and thermogravimetric (DTA–TG) analyses were carried out to determine the thermal characteristics and structural changes of synthesized compounds. DTA–TG analyses of the "precursor" of all samples were carried out in the temperature range from 30 to 1000 °C. The DTA–TG curves of BEZ and BGZ (representative) are shown in Fig. 5. The DTA–TG curves of both these samples are similar to each other. In the temperature range 50–100 °C, the observed weight loss (in TGA) and two endothermic peaks (in DTA) correspond to the elimination of residual water present in the precursor [23]. A second weight loss over the wide temperature range 250–450 °C is due to the decomposition and decarbonization of organic substances [24]. The strong exothermic peaks at 410 and 420 °C for BEZ and BGZ respectively in the DTA profiles also support this view. The weight loss above 600 °C is negligible which is in accordance with the phase formation obtained from powder XRD data. The broad exothermic peak observed at 820 °C for BEZ and 830 °C BGZ may probably be due to the decomposition of the product and rearrangement of the oxygen sublattice in disordered to ordered pyrochlore transition respectively [25]. The DTA–TG profiles of BSZ are similar to that of BEZ while the profiles of BLZ are quite different from other compounds under investigation. It shows a strong and broad endothermic peak in the range 300–750 °C with the center at 500 °C. The TGA of BLZ is characterized by slight weight loss up to 400 °C, marginal weight gain at 500 °C followed by continuous weight loss up to 800 °C. The reasons for such a behavior may be the stable phase formation of BLZ unlike other Bi containing pyrochlores.

3.3. Energy dispersive spectra (EDS)

Energy dispersive spectra were performed to confirm the composition of the obtained compounds. The EDS spectra of BLZ and BEZ prepared at 700 °C (representative) are shown in Fig. 6. From these EDS profiles, the area ratio of bismuth, lanthanide (Ln) and zirconium was found to be very close to 1:1:2 giving rise to a molecular formula of $BiLnZr_2O_7$ (Ln = La and Eu).

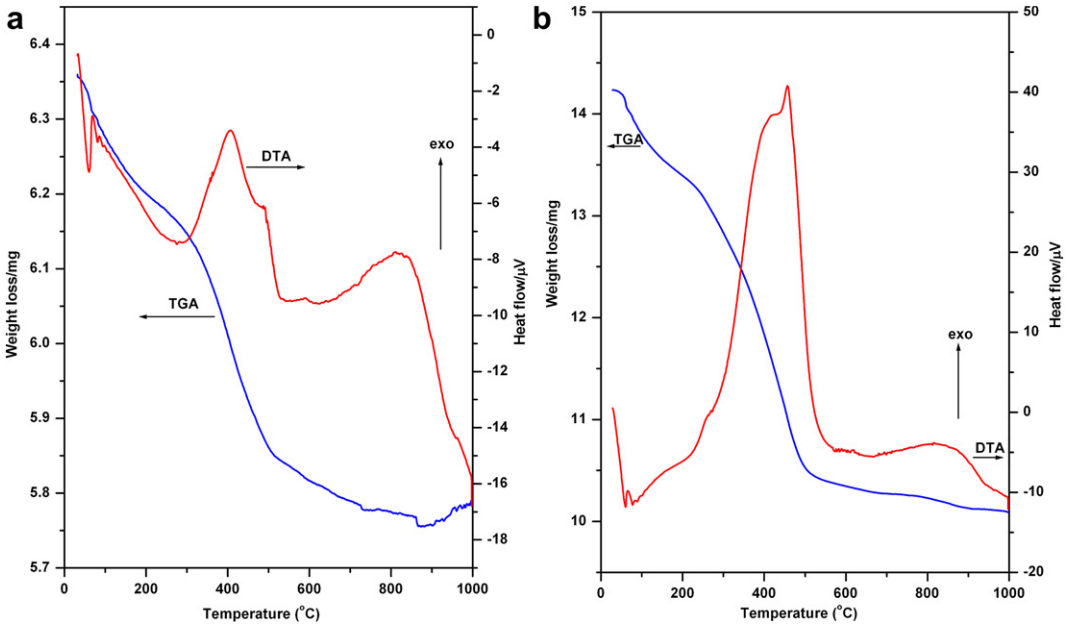

Fig. 5. DTA–TG profiles of (a) BEZ and (b) BGZ.

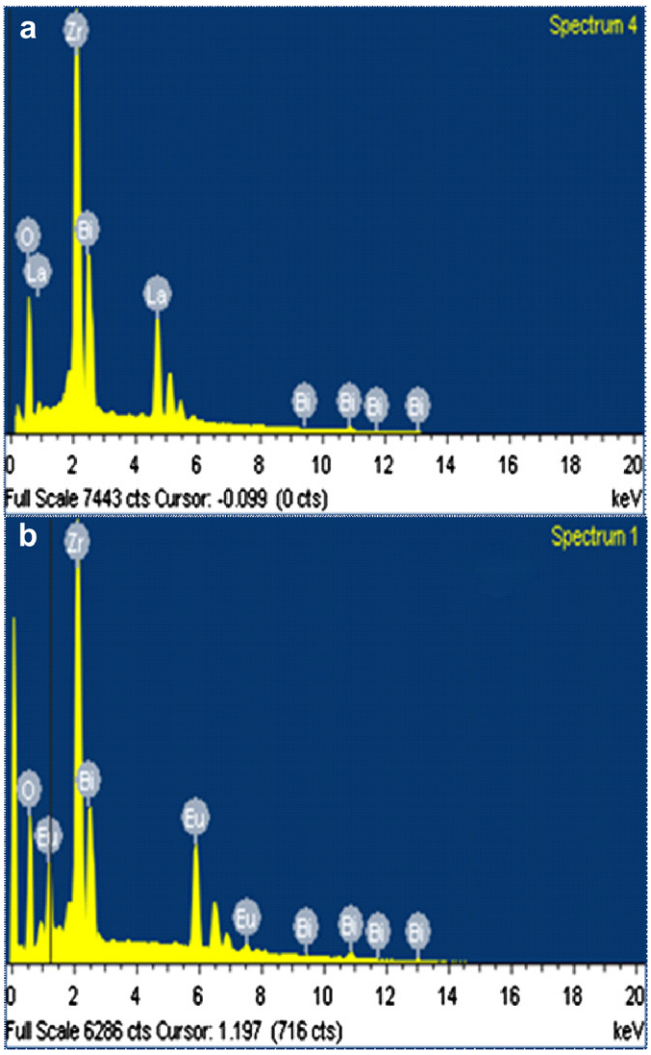

Fig. 6. Energy dispersive spectra of (a) BLZ and (b) BEZ.

3.4. Raman spectra

The Raman spectroscopic investigation gives the unequivocal information to distinguish the pyrochlore and defect fluorite structure of $A_2B_2O_7$ type materials. Therefore, in the present investigation the Raman spectra of all the samples calcined at different temperatures (500–700 °C) were recorded in the range 200–800 cm^{-1}. According to group theory analysis, cubic "pyrochlore $A_2B_2O_7$" belongs to space group (*Fd*-3*m*, O_h^7) with $Z = 8$ has six Raman active modes as [26,27]:

$$\Gamma = A_{1g} + E_g + 4F_{2g}$$

On the other hand, cubic "fluorite $A_2B_2O_7$" with the space group (*Fm*3*m*, O_h^5) and $Z = 4$, has only one Raman active mode:

$$\Gamma = F_{2g}$$

All the samples calcined at or below 700 °C gave broad Raman spectra. The broadness of Raman spectra may be due to (a) small crystallite size or (b) cation disorder in the system. Fig. 7a–d shows the Raman spectra of all the samples calcined at 700 °C. The Raman spectrum of BLZ is similar to that expected for "pyrochlore $A_2B_2O_7$" type oxides [28]. The most intense peak observed at 303 cm^{-1} was assigned to E_g while less intense peaks at 362, 568 and 643 cm^{-1} were due to F_{2g} modes. The weak band observed at 452 cm^{-1} was assigned to A_{1g} mode and the band observed at 713 cm^{-1} was due to combination band [26,27]. Thus, BLZ is crystallized in ordered pyrochlore structure. The Raman spectra of both BSZ and BEZ are also similar to those observed for ordered pyrochlore type oxides. However, the intensity of characteristic peak of ordered pyrochlore (303 cm^{-1}) is low and become very broad in BSZ and BEZ samples. Mandal et al. [29] have investigated detailed Raman and XRD studies of $Nd_{2-y}Gd_yZr_2O_7$ ($y = 0.0–2.0$). They have noticed that for $y \geq 1.8$ compositions, the bands observed at 305, 506 and 523 cm^{-1} have become broad with a decrease in intensity and the merger of the last two bands. Further, the value of x parameter of the 48f oxygen changes from 0.332(1) to 0.343(1) with a sudden change in the slope for the plot of x parameter versus y at $y = 1.8$. Based on these observations, they have concluded that the structure is transforming from "ordered pyrochlore" to "disordered pyrochlore" for compositions $y \geq 1.8$. In the present investigation, the broad Raman bands observed at ≈300 and ≈500–600 cm^{-1} for BSZ and BEZ samples may be due to structural transformation to "disordered pyrochlore" lattice. The Raman spectrum of BGZ is characterized by single broad band at ≈600 cm^{-1}. The intensity of characteristic band for ordered pyrochlore at ≈300 cm^{-1} is negligible. It is similar to that of reported $Gd_2Zr_2O_7$ (DF). These observations are consistent with their corresponding powder XRD results. The obtained Raman peak positions and their assignments for all the samples are given in Table 2.

3.5. UV–Vis diffuse reflectance spectra

Fig. 8 shows UV–Vis diffuse reflectance spectra (DRS) of BLnZ (Ln = La, Sm, Eu and Gd) compositions calcined at 700 °C. All the samples exhibit strong absorption in the range 200–400 nm. The absorption band edge of all the samples was determined by extrapolating the horizontal and sharply rising portions of the curves on to the wavelength axis and found to be around 420 nm. For a given oxide the absorption edge is strongly dependent on its crystallite size which is attributed to quantum size effects [30]. Accurate band gap energy of semiconducting oxide can be obtained from the plot of $(\alpha h\nu)^{1/2}$ versus $h\nu$ where α is absorption coefficient and $h\nu$ is photon energy. Extrapolation of linear portion of the plot to $(\alpha h\nu)^{1/2} = 0$ (i.e. onto x-axis) gives an estimation band gap energy. Absorbance versus photon energy also gives reasonable estimate of band gap energy. In the present investigation the band gap energy was calculated from the absorbance versus photon energy plot and found to be 2.8 eV for BLZ, BEZ, BGZ and 3.4 eV for BSZ. These values are comparable with the band gap energy of different forms of Bi_2O_3 [31–33].

3.6. Photocatalytic activity

The photocatalytic activity of BLnZ (Ln = La, Sm, Eu and Gd) (catalyst) was examined against the photo degradation of MO in aqueous solution under visible light irradiation. Experiments of photocatalysis in the presence of visible light were carried out (i) with only catalyst, (ii) with catalyst and H_2O_2, (iii) with only H_2O_2 and (iv) without catalyst and H_2O_2. The results are shown in Fig. 9. It is observed that the degradation of MO is 4% in the presence of only catalyst. However, in the presence of catalyst and 1 ml of 3% H_2O_2, the degradation of MO is increased substantially. The degradation of MO only in the presence of 1 ml of 3% H_2O_2 was negligible. The increase in the photocatalytic activity of BLnZ (Ln = La, Sm, Eu and Gd) in the presence of H_2O_2 can be attributed to the electron accepting nature of H_2O_2 leading to considerable

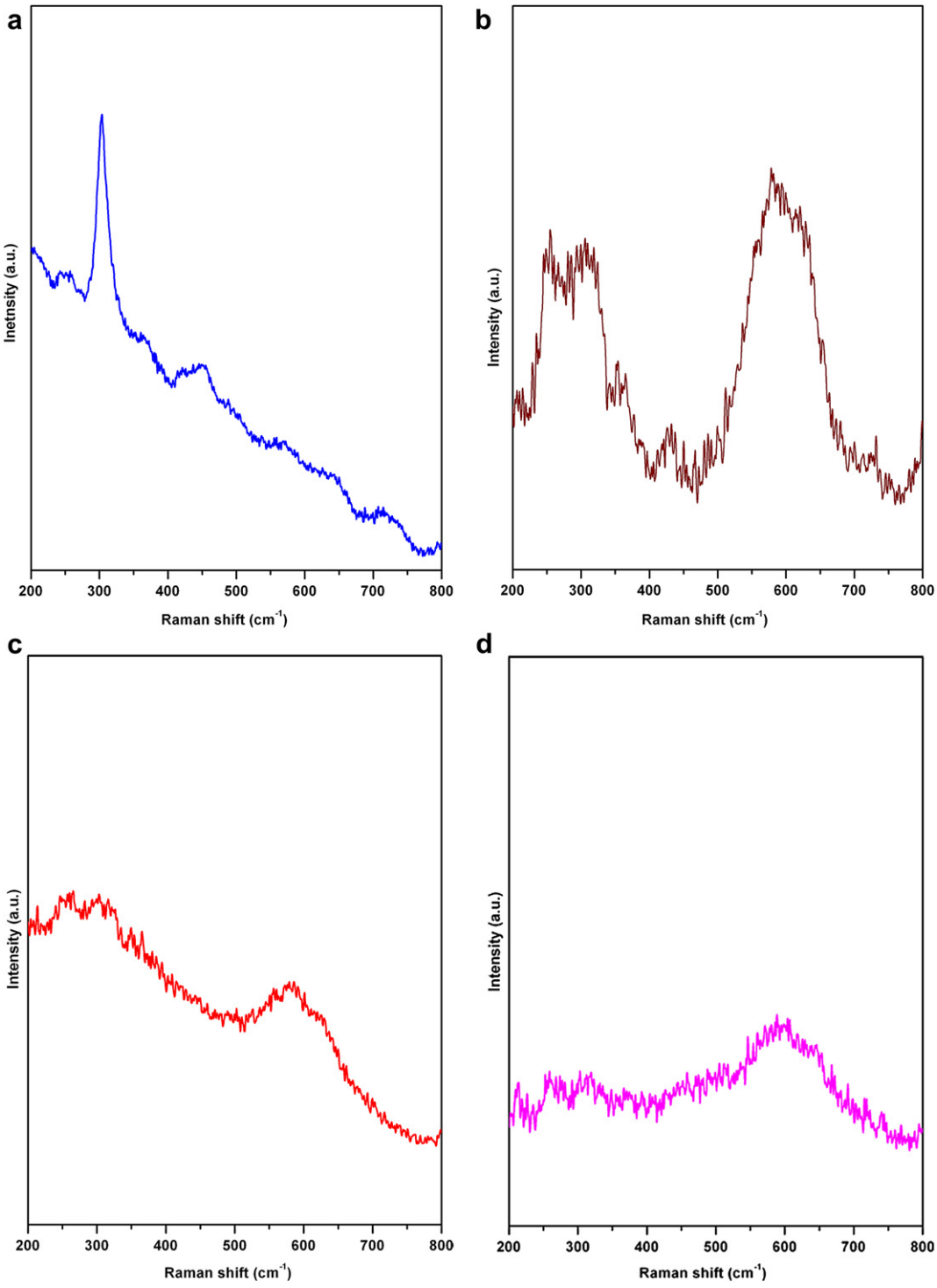

Fig. 7. Raman spectra of (a) BLZ, (b) BSZ, (c) BEZ and (d) BGZ.

decrease in the electron–hole recombination and oxidation of MO [34]. In the present investigation, the degradation of MO in the presence of H_2O_2 and catalyst was found to be 57%, 30%, 28% and 22% for BLZ, BSZ, BGZ and BEZ respectively. The photocatalytic activity studies of quaternary oxides are limited. Rosas Barrera et al. have reported the photocatalytic activity of Bi_2MNbO_7 (M = Al, Fe, Ga, In) films. The substitution effect of In^{3+} by Al^{3+} and Ga^{3+} on the structural and photocatalytic properties of Bi_2InNbO_7 was reported [35–37]. The photoactivity of a material is known to dependent on several factors such as surface structure, extent of crystallinity, surface area, structure of the material, ionic size, the adsorption ability of the pollutant, band gap energy of the material etc. $La_2Zr_2O_7$, which crystallizes in ordered pyrochlore structure, exhibits higher photoactivity while $Gd_2Zr_2O_7$ with defect fluorite structure shows less photoactivity [12,38]. The higher photocatalytic activity in the ordered pyrochlore may be due to increased mobility of electrons and oxygen vacancies through M–O–M bonds in the $A_2B_2O_7$ lattice [37]. Similarly, the higher photocatalytic

Table 2
Raman peak positions (cm^{-1}) and their assignments of BLZ, BSZ, BEZ and BGZ.

BLZ	BSZ	BEZ	BGZ	Assignment
303	307	306	–	E_g
362	354	350	–	F_{2g}
451	435	–	–	F_{2g}
568	580	587	–	F_{2g}
643	625	–	600	F_{2g}
713	730	–	–	Combination band

activity of Bi_2GaNbO_7 was attributed to its superior crystallinity [35]. A close examination of base lines of X-ray powder patters of BLnZ series shows that the crystallinity of BLZ, which crystallizes in ordered pyrochlore lattice, is highest compared to BGZ, BSZ and BEZ. In the present work, the higher photocatalytic activity of BLZ may be due to its higher crystallinity and ordered pyrochlore structure.

3.7. DC conductivity

The DC conductivity (σ_{dc}) of all the samples was obtained in the temperature range 130–700 °C. Its variation with temperature is shown in Fig. 10. The conductivity versus inverse temperature profiles can be divided into two regions based on the variation in slope. In the region I (130–340 °C), the change in conductivity with temperature is marginal with a small slope. The region II (340–700 °C) is characterized by a linear increase in conductivity with temperature having a higher slope. The observation of two slopes indicates two types of mechanisms for conduction in the temperature range 130–700 °C. As the electrical conductivity is a thermally activated process and follows Arrhenius equation given by

$$\sigma = \sigma_0 \exp\left(-\frac{E_a}{k_B T}\right)$$

where σ_0, E_a, k_B and T are pre-exponential factor, activation energy, Boltzmann constant and absolute temperature respectively. The activation energy (E_a) for conduction and pre-exponential factor (σ_0) are temperature independent. The pre-exponential factor is due to a combination of different effects i.e. defect states, complex defects, order and disorder states, lattice vibrations and impurity. The experimental data was fitted to the above equation. The activation energy and pre-exponential factor were calculated from the slope and intercept of the linear fits in the Arrhenius plots and the obtained values are given in Table 3. The magnitude of conductivity for all the samples in the region I (130–340 °C) is in the range 10^{-6}–10^{-7} S m^{-1} with an activation energy E_a of ~0.13–0.02 eV. Similarly, the conductivity in the region II (340–700 °C) is in the range 10^{-3}–10^{-4} S m^{-1}, associated with an activation energy, E_a, of ~1.14–1.27 eV.

The discussion pertaining to mechanism of conduction in bismuth based pyrochlores is limited [39,40]. The variation of conductivity with temperature clearly shows two types of mechanisms. In the region I, the magnitude of activation energy suggest that hopping of defect related weakly bonded electrons are responsible for conduction [40]. The framework structure of $A_2B_2O_7$ may not permit the mobility of oxygen ions in this temperature range leading to a lower conductivity. It was reported that the

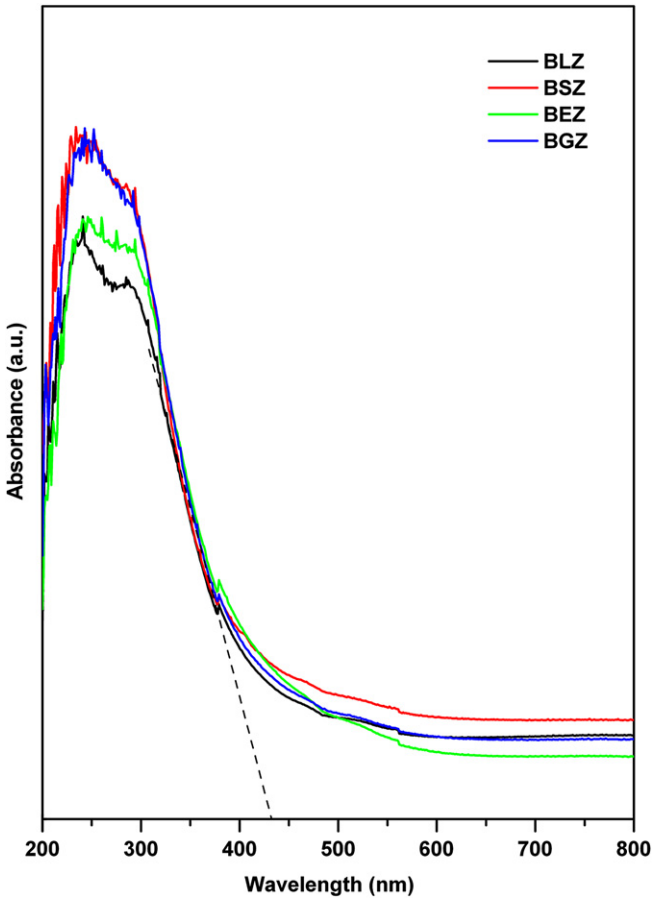

Fig. 8. UV–Vis diffuse reflectance spectra of BLZ, BSZ, BEZ and BGZ.

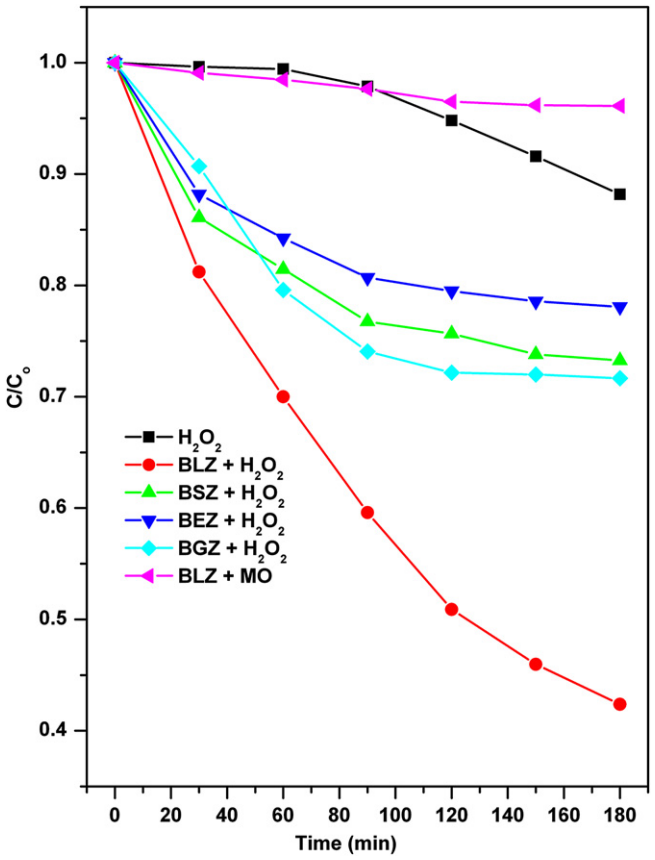

Fig. 9. Photocatalytic degradation of methyl orange loaded with different catalysts.

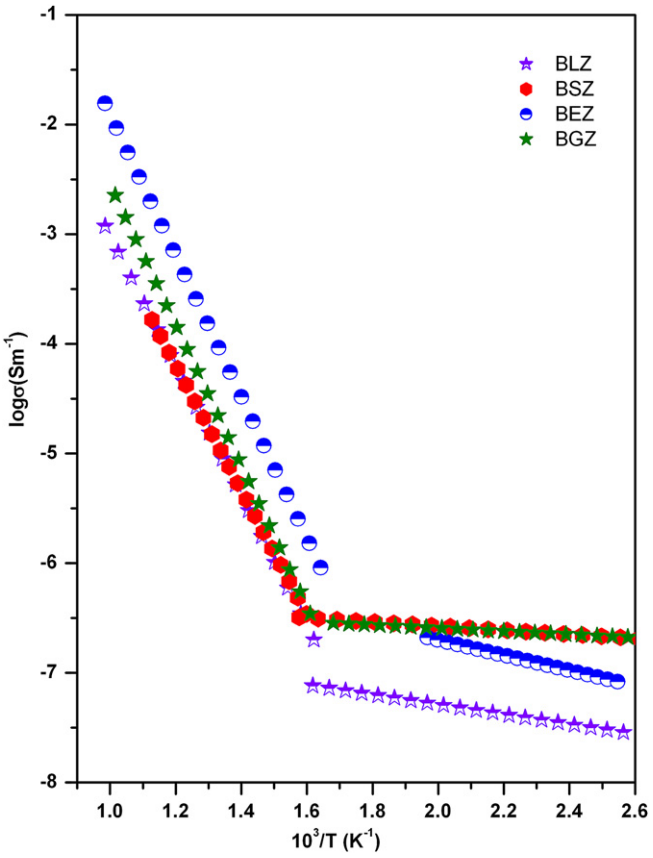

Fig. 10. Arrhenius plots of Dc (logσ) conductivity as a function of reciprocal temperature.

Table 3
Activation energy and pre-exponential factor of BLZ, BSZ, BEZ and BGZ.

Compound	Activation energy (eV)	Pre-exponential factor (S m^{-1})	Conductivity at 700 °C (S m^{-1})
BLZ	1.170	8.15×10^2	7.10×10^{-4}
BSZ	1.142	5.47×10^2	9.85×10^{-4}
BEZ	1.275	3.46×10^4	8.60×10^{-3}
BGZ	1.270	7.54×10^2	7.50×10^{-4}

threshold activation energy for oxide ion conduction is ~1 eV [41–43]. The relatively high activation energy (~1.31 eV) observed in the region II (340–700 °C) indicate that the conduction is due to hopping of oxide ions through channels of 48f sites [44]. The magnitude of conductivity at 700 °C is in the range 10^{-3}–10^{-4} S m^{-1} which is two orders lower than those observed for related systems [45]. The reason for lower conductivity may be due to its poor stability.

4. Conclusions

Quaternary oxides belonging to pyrochlore family of compositions $BiLnZr_2O_7$ (Ln = La, Sm, Eu and Gd) were prepared by sol–gel method. BLZ and BGZ were crystallized in ordered pyrochlore and defect fluorite lattice respectively. Both BSZ and BEZ were crystallized in disordered pyrochlore lattice but unstable above 700 °C and decompose to $Bi_{7.38}Zr_{0.62}O_{12.31}$, $Ln_{0.2}Zr_{0.8}O_{1.9}$ and Ln_2O_3 (Ln = Sm and Eu). The Raman spectra of BLZ, BEZ, BSZ and BGZ are consistent with powder XRD results. The band gap energies of all the compositions were found to be in the range 2.85–3.2 eV and comparable with the band gap energy of Bi_2O_3. All the samples exhibit good photocatalytic activity under visible light. BLZ shows highest photocatalytic activity among the samples under investigation. The relatively high photocatalytic activity of BLZ may be due to the higher crystallinity and ordered pyrochlore structure. The variation of conductivity with temperature (130–700 °C) clearly shows two types of mechanism. The lower conductivity observed in the temperature range 130–340 °C is due to the weakly bonded electrons while the higher conductivity noticed in the temperature range 340–700 °C is due to hopping of oxide ions through channels of 48f sites.

Acknowledgments

This work was supported by University Grants Commission (UGC), New Delhi under Grant no: 37-288/2009 (SR). One of the authors (BVK) thanks Council of Scientific and Industrial Research, New Delhi for the award of Senior Research Fellowship (CSIR-SRF).

References

[1] M.A. Subramanian, Aravamudan, G.V. Subba Rao, Oxide pyrochlores – a review, Prog. Solid State Chem. 15 (1983) 55–143.
[2] I. Levin, T.G. Amos, J.C. Nino, T.A. Vanderah, C.A. Randall, M.T. Lanagan, J. Solid State Chem. 168 (2002) 69–75.
[3] M. Avdeev, M.K. Haas, J.D. Jorgensen, R.J. Cava, J. Solid State Chem. 169 (2002) 24–34.
[4] R.D. Shannon, Acta Crystallogr. Sect. A 32 (1972) 751–767.
[5] B.J. Kennedy, Mater. Res. Bull. 32 (1997) 479–483.
[6] J.C. Nino, Ph.D Thesis, The Pennsylvania State University, 2002.
[7] M.T. Lanagan, D. Anderson, A. Baker, J.C. Nino, S. Perini, C.A. Ran-dall, T.R. Shrout, T. Sogabe, H. Youn, in: Proceedings of the International Symposium on Microelectronics, IMAPS, Baltimore, MD, 2001.
[8] S.W. Wang, W. Lu, N. Li, Z.F. Li, H. Wang, M. Wang, X.C. Shen, Mater. Res. Bull. 37 (2002) 1691–1697.
[9] S.W. Wang, H. Wang, S. Shang, J. Huang, Z. Wang, M. Wang, J. Cryst. Growth 217 (2000) 388–392.
[10] S.W. Wang, H. Wang, X. Wu, S. Shang, M. Wang, Z. Li, W. Lu, J. Cryst. Growth 224 (2001) 323–326.
[11] A.T. Ashcroft, A.K. Cheethan, M.L.H. Green, C.P. Grey, P.D.F. Vernon, J. Chem. Soc. Chem. Commun. (1989) 1667–1669.
[12] J.M. Sohn, M.R. Kim, S.I. Woo, Catal. Today 83 (2003) 289–297.
[13] S. Liang, L. Shen, J. Zhu, Y. Zhang, X. Wang, Z. Li, L. Wu, X. Fu, RSC Adv. 1 (2011) 458–467.
[14] S. Liang, S. Zhu, J. Zhu, Y. Chen, Y. Zhang, L. Wu, Phys. Chem. Chem. Phys. 14 (2012) 1212–1222.
[15] H. Kato, K. Asakura, A. Kudo, J. Am. Chem. Soc. 125 (2003) 3082–3089.
[16] J. Bi, L. Wu, J. Li, Z. Li, X. Wang, X. Fu, Acta Mater. 55 (2007) 4699–4705.
[17] L. Wu, J. Bi, Z. Li, X. Wang, X. Fu, Catal. Today 131 (2008) 15–20.
[18] R. Chen, J. Bi, L. Wu, Z. Li, X. Fu, Cryst. Growth Des. 9 (2009) 1775–1779.
[19] A.J. Burggraaf, T. van Dijk, M.J. Verkerk, Solid State Ion. 17 (1985) 519–522.
[20] A.L. Hector, S.B. Wiggin, J. Solid State Chem. 177 (2004) 139–145.
[21] J. Bassett, R.C. Denney, G.H. Jeffery, J. Mendham (Eds.), Vogel's Text Book of Quantitative Inorganic Analysis, fourth ed., (1978), pp. 455–456. London.
[22] A.R. West, Solid State Chemistry and its Applications, Wiley, New York, 1974, p. 172.
[23] Y. Ohara, K. Koumoto, T. Shimizu, H. Yanagida, J. Mater. Sci. 30 (1995) 263.
[24] S. Doeuff, M. Henry, C. Sanchez, Mater. Res. Bull. 25 (1990) 1519–1529.
[25] A.V. Shlyakhtina, J.C.C. Abrantes, L.L. Larina, L.G. Shcherbakova, Solid State Ion. 176 (2005) 1653–1656.
[26] M.T. Vandenborre, E. Husson, J.P. Chatry, D. Michel, J. Raman Spectrosc. 14 (1983) 63–71.
[27] H.C. Gupta, Sonal Brown, Neelima Rani, V.B. Gohel, J. Raman Spectrosc. 32 (2001) 41–44.
[28] B. Vijaya Kumar, Radha Velchuri, G. Prasad, B. Sreedhar, K. Ravikumar, M. Vithal, Ceram. Inter. 36 (2010) 1347–1355.
[29] B.P. Mandal, Ankita Banerji, Vasant Sathe, S.K. Deb, A.K. Tyagi, J. Solid State Chem. 180 (2007) 2643–2648.
[30] B. Vijaya Kumar, Radha Velchuri, V. Rama Devi, G. Prasad, B. Sreedhar, C. Bansal, M. Vithal, J. Appl. Phys. 108 (2010) 044906.
[31] H. Gobrecht, S. Seeck, H.E. Bergt, A. Martens, K. Kossmann, Phys. Stat. Sol. 33 (1969) 599–606.
[32] V. Dolocan, Appl. Phys. 16 (1978) 405–407.
[33] W. Xiaohong, Q. Wei, H. Weidong, J. Mol. Catal. A 263 (2006) 167–171.
[34] P.X. Lei, C.C. Chen, J. Yang, W.H. Ma, J.C. Zhao, L. Zang, Environ. Sci. Technol. 39 (2005) 8466–8474.
[35] K.L. Rosas-Barrera, J.L. Ropero-Vega, J.A. Pedraza-Avella, M.E. Nino-Gomez, J.E. Pedraza-Rosas, D.A. Laverde-Catano, Catal. Today 166 (2011) 135–139.

[36] J.L. Ropero-Vega, K.L. Rosas-Barrera, J.A. Pedraza-Avella, D. Laverde-Catano, J.E. Pedraza-Rosas, M.E. Nino-Gómez, Mater. Sci. Eng. B 174 (2010) 196–199.
[37] Z. Zou, J. Ye, H. Arakawa, Chem. Mater. 13 (2001) 1765–1769.
[38] Y. Tong, J. Zhu, L. Lu, X. Wang, X. Yang, J. Alloys Compd. 465 (2008) 280–284.
[39] H. Du, X. Yao, H. Wang, Appl. Phys. Lett. 88 (2006) 212901.
[40] Huiling Du, Xiang Shi, Yu Cui, Solid State Commun. 159 (2010) 1213–1216.
[41] B.P. Dasa, R.N.P. Choudhary, P.K. Mahapatra, Mater. Sci. Eng. B 104 (2003) 96–105.
[42] W. Li, K. Chen, Y. Yao, J. Zhu, Y. Wang, Appl. Phys. Lett. 85 (2004) 4717.
[43] Z.Y. Wang, T.G. Chen, Phys. Stat. Sol. A 167 (1998) R3–R4.
[44] P.J. Wilde, C.R.A. Catlow, Solid State Ion. 112 (1998) 173–183.
[45] H. Yamamura, H. Nishino, K. Kakinuma, K. Momura, Solid State Ion. 158 (2003) 359–365.